

# UCLA

## UCLA Previously Published Works

### Title

Analysis of Saturation Recovery Amplitudes to Characterize Conformational Exchange in Spin-Labeled Proteins

### Permalink

<https://escholarship.org/uc/item/0j47t1p7>

### Journal

Applied Magnetic Resonance, 48(11-12)

### ISSN

0937-9347

### Authors

Bridges, Michael D  
Yang, Zhongyu  
Altenbach, Christian  
[et al.](#)

### Publication Date

2017-12-01

### DOI




10.1007/s00723-017-0936-3

### Copyright Information

This work is made available under the terms of a Creative Commons Attribution License, available at <https://creativecommons.org/licenses/by/4.0/>

Peer reviewed

# Analysis of Saturation Recovery Amplitudes to Characterize Conformational Exchange in Spin-Labeled Proteins

Michael D. Bridges<sup>1</sup>  · Zhongyu Yang<sup>1,2</sup>  ·  
Christian Altenbach<sup>1</sup> · Wayne L. Hubbell<sup>1</sup> 

Received: 4 August 2017 / Revised: 23 August 2017 / Published online: 5 October 2017  
© Springer-Verlag GmbH Austria 2017

**Abstract** Analysis of saturation recovery data from spin-labeled proteins is extended to include the amplitudes in addition to the recovery rates for two-site exchange. It is shown that the recovery amplitudes depend strongly on the exchange rate between states as well as their populations and this dependence provides a simple criterion to identify exchange rates in the 10–1000 kHz range. Analysis of experimental SR relaxation curves via the uniform penalty (UPEN) method allows for reliable identification of single, double, or other multiple-component traces, and global fitting of a set of relaxation curves using both relaxation rates and amplitudes determined from the UPEN fits allows for the estimation of exchange rate in the above domain. The theory is tested on simple model systems, and applied to the determination of conformational exchange rates in spin-labeled mutants of T4 Lysozyme and intestinal fatty acid binding protein. Finally, an example of  $T_1$ -weighted spectral editing is provided for systems in the slow exchange limit.

## 1 Introduction

Structural fluctuations of proteins on ps–ms timescales are fundamental to protein function, and may account for allostery [1, 2], promiscuity of protein–protein interactions [3, 4] and rapid kinetics of protein–protein recognition/binding [5, 6], as well as playing a key role in the evolution of protein function [7]. To reveal the role of protein dynamics in function, it is essential to have experimental tools to explore

---

✉ Wayne L. Hubbell  
hubbellw@jsei.ucla.edu

<sup>1</sup> Jules Stein Eye Institute and Department of Chemistry and Biochemistry, UCLA School of Medicine, University of California, Los Angeles, CA 90095-7008, USA

<sup>2</sup> Present Address: Department of Chemistry and Biochemistry, North Dakota State University, Fargo, ND 58102, USA

both the amplitude and timescales of motion under near-physiological conditions. Site-directed spin labeling (SDSL) electron paramagnetic resonance (EPR) spectroscopy using the nitroxide side chain R1 (Fig. 1) is well suited to report on protein motions on the ps– $\mu$ s timescale regardless of system size or complexity, including membrane proteins in their native lipid environment [8]. Continuous wave (CW) EPR spectra are sensitive to motions of the nitroxide in the time window of ps–ns, which corresponds to backbone fluctuations in proteins. Thus, CW spectra of R1 can directly reveal backbone dynamic disorder and estimate the amplitude of motion [9–11]. However, the spectra contain no information on dynamics in the important  $\mu$ s–ms range characteristic of conformational exchange, as this is far removed from the ps–ns time window of CW EPR spectroscopy. On the other hand, pulse saturation recovery (SR) and electron–electron double resonance (ELDOR) EPR of R1 in proteins can reveal dynamics on the  $\approx$  1–70  $\mu$ s timescale [12, 13], allowing for characterization of structural fluctuations and conformational exchange in proteins in a time domain challenging for other spectroscopic techniques [14].

Pulse SR EPR, developed largely by Hyde in the 1970s, employs a weak CW microwave source to measure the recovery of longitudinal magnetization to Boltzmann equilibrium following a high-power saturating pulse (Fig. 2) [15, 16]. The characteristic exponential recovery time for a single population of R1 in a protein is the spin lattice relaxation time,  $T_1$ .  $T_1$ s of nitroxide spin labels are typically in the range from 1 to 10  $\mu$ s and depend on the rotational correlation time of the nitroxide side chain in the investigated range of  $\approx$  0.1–10 ns [12, 17]. Importantly, the CW EPR spectra of R1 in proteins also depend on motions in this time range that originate in part from internal dynamic modes of the side chain [10]. Modulation of these internal modes by interactions of the side chain with the local protein structure is thus reflected both in the EPR spectra and  $T_1$ . For example, if R1 is located at a protein site where it has strong interactions with the surrounding side chains or backbone, the CW spectrum will reflect the immobilization with broad spectral components and the  $T_1$  will typically be  $\geq$  7  $\mu$ s. On the other hand, in the absence of such interactions the spectrum will be characterized by narrow CW resonance lines and  $T_1 \leq$  3  $\mu$ s [12].

Now consider a protein fluctuating between two conformational substates  $\alpha$  and  $\beta$  on the  $\mu$ s–ms timescale, and with an R1 residue placed at a site where it experiences different interactions in the two states. In view of the above considerations, the CW EPR spectrum will reveal the existence of the two conformations by a two-

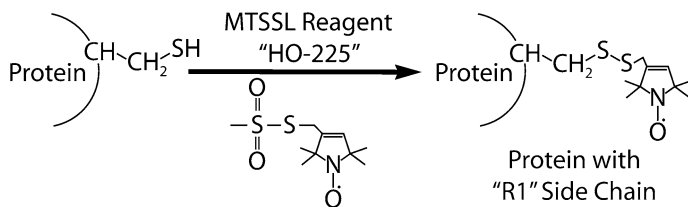


**Fig. 1** Site-directed spin labeling and the R1 side chain. The number of favorable rotamers and internal modes of the nitroxide side chain are highly restricted due to the interaction of the disulfide with the backbone in the case of loops and helices [40]

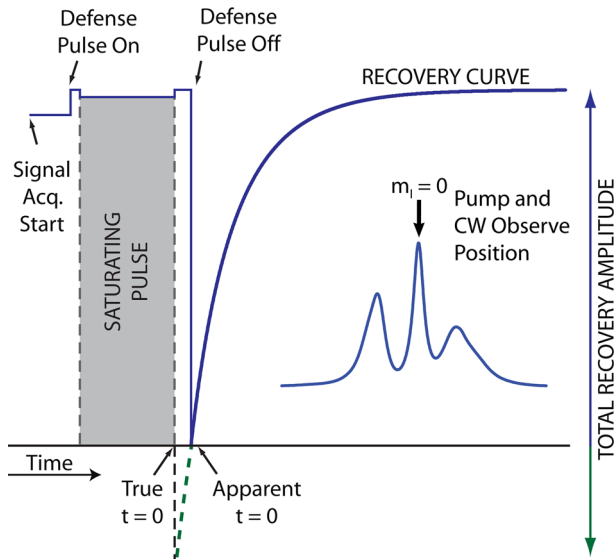


**Fig. 2** Long-pulse saturation recovery. An excitation (“pump”) pulse located at the field position of maximum intensity in the EPR absorption spectrum (see *inset*) causes saturation of the electron spin system. Low-power CW detection (“CW observe”) at the same field position records the exponential signal recovery. The “defense pulse” is required to protect the detector electronics, and as such, the earliest time-points of the recovery signal that begin at the “true”  $t = 0$  are not recorded

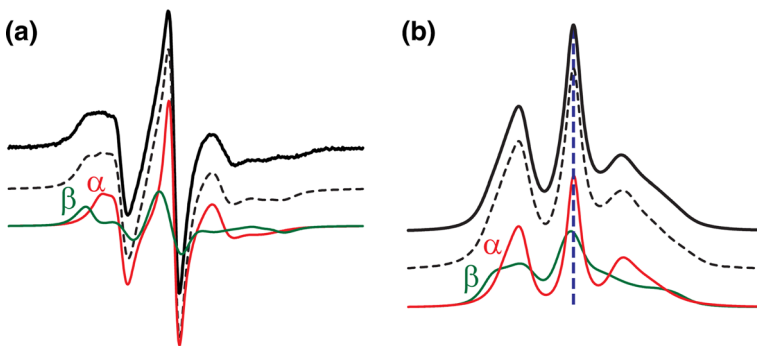


**Fig. 3** Conformational equilibrium revealed in CW EPR spectra. **a** A two-component first-derivative EPR spectrum (*top black trace*) of a spin-labeled protein in which the nitroxide experiences different interactions in two conformations in slow or intermediate exchange. The fast motion (*bottom red,  $\alpha$* ) and slow motion (*bottom green,  $\beta$* ) traces are the individual components resolved by spectral simulations and the *dashed black (middle)* trace is the total simulation lineshape. **b** The corresponding absorption spectra obtained by integration. Note that the magnetic field at maximum absorption of the two components is offset due to differing effective  $g$ -tensors of the two dynamic components (color figure online)

component lineshape (Fig. 3). Averaging of the  $\alpha$  and  $\beta$  spectral components will only occur with exchange on a timescale short compared to the difference in their spectral frequencies, which is typically only a few nanoseconds for X-band EPR (i.e., an order of magnitude or more shorter than the conformational exchange

timescale) [18]. In principle, spectral averaging could occur due to rotational diffusion of the entire protein, but for proteins of molecular weight greater than 30 kD, the rotational correlation times are too long to produce complete spectral averaging.

The intrinsic  $T_1$ s of the nitroxide in these two motional states will be different and the saturation recovery signal detected at the center line (spectral absorption maximum) of the spin label will in general be bi-exponential. Differentiating bi-exponential from mono-exponential saturation recovery curves—particularly in cases of poor signal-to-noise—can be challenging. One strategy involves fitting the SR data to a selected model that has one, two, or more exponentials and evaluating the residual trace (e.g., see Figs. 7c, 8c of Ref. [12]). An alternative approach is the uniform penalty (UPEN) method [19, 20] which has been extensively used in fitting NMR relaxation data (for example, [21, 22]) and more recently for analyzing EPR relaxation data from SR [23]. UPEN fits the experimental recovery curve to a set of differentially weighted exponential recovery curves across a range of  $T_1$ s. The fitting output is a band-limited semi-continuous distribution of relaxation time constants used to generate the recovery data. Thus, UPEN analysis produces a distribution of relaxation times without preexisting assumptions regarding the number of exponentials or functional form of the distributions; as such, it is a ‘model-free’ fit [19, 20]. High signal-to-noise ( $S/N$ ) is important in any analysis of exponential data. The  $S/N$  of an SR relaxation increases with increasing power of the observing CW microwave source, but at the expense of perturbation of the relaxation rates [24]. However, relative component amplitudes are found to be independent of observing power for the powers employed in this study.

In the present study, UPEN analysis is employed to analyze high  $S/N$  ( $>100$ ) SR curves obtained from spin-labeled proteins. For the systems studied here, bi-exponential relaxations are expected (but not assumed). Indeed, all relaxation curves obtained are well-fit with two relatively narrow distributions of effective  $T_1$ s, and the area of each distribution is proportional to the relaxation amplitude of the corresponding component. The inclusion of amplitude data in the analysis is a novel aspect of this study, and proves to provide a more robust fitting for extracting exchange rates than the use of relaxation rate data alone. Allowing for distributions of  $T_1$ s rather than discrete values is physically realistic considering the microscopic heterogeneity of the local environment around the nitroxide in any conformation. However, the distribution widths resulting from UPEN fits are influenced by the choice of penalty parameters, and no attempt is made to relate them to details of the structure, nor are they employed in any aspect of the analysis (see Sect. 6).

## 2 The Two-Site Exchange Model

Consider again the aforementioned two-substate fluctuating protein, which explores the exchange equilibrium  $\alpha \leftrightarrow \beta$ . The expected forward and reverse rate constants  $k_{\alpha\beta}$  and  $k_{\beta\alpha}$  are related to the average exchange lifetime  $\tau_{ex}$  according to  $\tau_{ex} = (k_{\alpha\beta} + k_{\beta\alpha})^{-1}$ . In the limit of slow exchange on the nitroxide  $T_1$  timescale, the exhibited time constants of the two exponential recoveries are simply the

intrinsic spin lattice relaxation times of the two nitroxide states,  $T_{1\alpha,0}$  and  $T_{1\beta,0}$ , as  $\tau_{\text{ex}}^{-1} \ll \frac{1}{2} [T_{1\alpha,0}^{-1} - T_{1\beta,0}^{-1}]$ .

In the fast exchange limit where  $\tau_{\text{ex}}^{-1} \gg \frac{1}{2} [T_{1\alpha,0}^{-1} - T_{1\beta,0}^{-1}]$ , the relaxation is a single exponential with a weighted average recovery constant defined by  $\frac{1}{T_{\text{eff}}} = \frac{f_{\alpha}}{2T_{1\alpha,0}} + \frac{1-f_{\alpha}}{2T_{1\beta,0}}$ , where  $f_{\alpha}$  is the fractional population of the  $\alpha$  state. Note that simple rotameric exchange of R1 can give rise to multicomponent CW-EPR spectra, but apparently lies in the fast limit ( $\tau_{\text{ex}} \leq 1 \mu\text{s}$ ), and so it is distinguishable from true conformational exchange by SR-EPR [12].

In the intermediate case where  $\tau_{\text{ex}}^{-1} \approx \frac{1}{2} [T_{1\alpha,0}^{-1} - T_{1\beta,0}^{-1}]$ , it was shown that analysis of time constants from a set of saturation recovery curves obtained in the presence of different concentrations of a paramagnetic relaxation reagent (RA) could be used to confirm intermediate exchange, and under ideal conditions, estimate the exchange lifetime [12]. The purpose of the exchange reagent is to vary the apparent relaxation times for the nitroxide via Heisenberg exchange (HE), which differentially shortens the relaxation rates by an amount equal to the collision rate of the nitroxide with the RA. The nitroxide side chains in states  $\alpha$  and  $\beta$  generally have different solvent accessibilities, and hence different HE rates for a given concentration of RA. This general strategy was introduced by Kusumi et al. [27] for analysis of lipid exchange between membrane domains. In principle, this approach provides a sufficiently large data set to extract exchange rates from the set of unknown parameters that include the intrinsic  $T_{1\text{s}}$ , the apparent solvent accessibilities of the nitroxide in each state, and the exchange lifetime. The theoretical hallmark of intermediate exchange is a nonlinearity in the plot of measured relaxation rates vs. RA concentration, but the curvature in such plots is very subtle and the method is only useful for reliable quantitation of exchange rates with extremely high quality data over a large range of RA concentrations. Nevertheless, SR data were shown to clearly discriminate fast from slow and intermediate exchange, which is important for distinguishing R1 rotameric exchange from protein fluctuations [12].

A main result of the present analysis is that in general SR amplitudes are not only functions of the populations of states, but also of the exchange rate constant and the RA concentration, and that the RA concentration dependence of the amplitude provides a simple and robust means of identifying cases of intermediate exchange on the  $\mu\text{s}$  timescale. SR amplitudes and rates are shown to have different dependencies on RA concentration, and using both relative area and rate data in a global fitting procedure of UPEN-analyzed SR data at various RA concentrations introduces additional constraints on fitting parameters that allow a significantly more reliable determination of exchange rates.

### 3 Theoretical Considerations

#### 3.1 Inclusion of Relaxation Amplitudes in SR Exchange Measurements

In the following, modifications of the basic equations for saturation recovery curves are introduced to account for the amplitudes of the recovery signal as well as the

rates. This derivation follows that given in Bridges, Hideg and Hubbell (hereafter referred to as “BHH”), except for the inclusion of quantities that relate signal amplitudes to spectral lineshape, and the reader is referred to that publication for details [12]. For an analysis that includes experimental recovery amplitudes, it is essential that complete saturation of the spin system be achieved by the pump pulse, and that the time origin of the recovery curves be referenced to the true zero, immediately following termination of a pump pulse (see Sect. 4 and Fig. 2); all expressions given below assume this to be the case.

As in BHH, we consider exchange between two protein conformations  $\alpha$  and  $\beta$  in which the nitroxide has resolved spectral components. The  $\{1/2, -1/2\}$  spin states of the unpaired nitroxide electron in conformations  $\alpha$  and  $\beta$  are labeled  $\{1, 2\}$  and  $\{3, 4\}$ , respectively. In the SR experiment, the saturating and observing frequencies are at the same position in the central resonance line ( $m_I = 0$ ) of the nitroxide, where both  $\alpha$  and  $\beta$  resonances overlap but with a small offset due to different effective  $g$  factors of the nitroxides (Fig. 3 and caption). The saturation recovery signal recorded at this position will thus have contributions from nitroxides in both states, the intensities of which are proportional to the corresponding population differences between the spin states:

$$i_\alpha = l_\alpha \{ (n_1 - n_2) - (N_1 - N_2) \}, \quad (1)$$

$$i_\beta = l_\beta \{ (n_3 - n_4) - (N_3 - N_4) \}, \quad (2)$$

where  $n_i$  and  $N_i$  are the instantaneous and equilibrium numbers of spins per unit volume, and  $l_\alpha$  and  $l_\beta$  are the empirical constants for a given field position and a given set of instrumental parameters that relate the spin concentration to the spectral intensity. Note that  $l_\alpha$  and  $l_\beta$  will differ due to resonance lineshape differences, e.g., a broad resonance line will have a lower intensity than a narrow line for the same number of spins.

The total saturation recovery signal is

$$i_{\text{SR}} = \rho_1 i_\alpha + \rho_2 i_\beta, \quad (3)$$

where  $\rho_1$  and  $\rho_2$  are the fractions of maximum signal amplitude contributed at the observe field position by the  $\alpha$  and  $\beta$  spin populations. These two parameters account for the offset of individual resonance maxima relative to an arbitrary observe position. Thus, combining (1) through (3),

$$i_{\text{SR}} = \rho_1 l_\alpha \{ (n_1 - n_2) - (N_1 - N_2) \} + \rho_2 l_\beta \{ (n_3 - n_4) - (N_3 - N_4) \}. \quad (4)$$

With these modifications and by following the derivations presented in BHH, the SR signal is

$$i(t) = A_f e^{-(X+Y+Z)t} + A_s e^{-(X+Y-Z)t}, \quad (5)$$

where the relaxation rate constant for the first term ( $X + Y + Z$ ) is larger than that for the second ( $X + Y - Z$ ); each recovery component is preceded by a pre-exponential amplitude,  $A_f$  (fast state,  $\alpha$ ) and  $A_s$  (slow state,  $\beta$ ), respectively. Contained within these terms are the experimentally determined spin lattice relaxation rate constants ( $W_\alpha, W_\beta$ ), the mole fractions of states  $\alpha$  and  $\beta$  ( $f_\alpha, f_\beta$ ), the exchange rate

constant ( $k$ ), a Boltzmann population ratio ( $c$ ), the total spin concentration ( $C_{\text{tot}}$ ), and the aforementioned parameters  $l_\alpha$ ,  $l_\beta$ ,  $\rho_1$ , and  $\rho_2$ . Assuming complete saturation at time  $t = 0$  after the pulse, the above terms are explicitly defined by

$$A_f = -\left(\delta + \frac{\gamma}{Z}\right), \tag{6}$$

$$A_s = -\left(\delta - \frac{\gamma}{Z}\right), \tag{7}$$

$$\delta = \left(\frac{cC_{\text{tot}}}{2}\right) (\rho_1 l_\alpha f_\alpha + \rho_2 l_\beta f_\alpha (1 - f_\alpha)), \tag{8}$$

$$\gamma = \left(\frac{cC_{\text{tot}}}{2}\right) [(X - Y)(\rho_1 l_\alpha f_\alpha - \rho_2 l_\beta f_\alpha (1 - f_\alpha)) - 2k((\rho_1 l_\alpha + \rho_2 l_\beta) f_\alpha (1 - f_\alpha))], \tag{9}$$

$$c = \frac{1 - b}{1 + b}, \tag{10}$$

$$X = W_\alpha + k(1 - f_\alpha), \tag{11}$$

$$Y = W_\beta + k f_\alpha, \tag{12}$$

$$Z = \sqrt{(W_\alpha - W_\beta)^2 + 2k(W_\alpha - W_\beta)(1 - 2f_\alpha) + k^2}, \tag{13}$$

$$k = \frac{1}{2}(k_{\alpha\beta} + k_{\beta\alpha}), \tag{14}$$

where for Eq. (10)  $b_\alpha = \frac{N_2}{N_1} = e^{-(E_2 - E_1)/RT}$ ,  $b_\beta = \frac{N_4}{N_3} = e^{-(E_4 - E_3)/RT}$ , and  $b_\alpha \approx b_\beta \approx$  “b”.

Equations (6) through (14) are the same as those given in BHH, except for the inclusion of the lineshape parameters  $l_\alpha$  and  $l_\beta$  in Eqs. (8) and (9) that contribute to the recovery amplitudes. In BHH, lineshape differences between states  $\alpha$  and  $\beta$  were ignored, and the simplification  $\rho_1 = \rho_2 = 1$  was made. This had no consequences for the conclusions of that study because for the analysis of SR rates alone lineshape differences and degree of spectral overlap are unimportant (i.e.,  $l_\alpha$ ,  $l_\beta$ ,  $\rho_1$ , and  $\rho_2$  do not appear in the experimentally determined exponential time constants). However, for the analysis of amplitudes this assumption is clearly not valid.

In the presence of an added relaxation reagent, the spin–lattice relaxation rates ( $W_\alpha$ ,  $W_\beta$ ) and relaxation times ( $T_{1\alpha,RA}$ ,  $T_{1\beta,RA}$ ) are dependent on the intrinsic constants ( $W_{\alpha,0}$ ,  $W_{\beta,0}$ ,  $T_{1\alpha,0}$ ,  $T_{1\beta,0}$ ), the concentration of RA, and the accessibility of each site to the RA ( $j_{\alpha,RA}$ ,  $j_{\beta,RA}$ ), i.e.,

$$W_\alpha = (2T_{1\alpha,RA})^{-1} = (2T_{1\alpha,0})^{-1} + j_{\alpha,RA}[\text{RA}] = W_{\alpha,0} + j_{\alpha,RA}[\text{RA}], \tag{15}$$

$$W_\beta = (2T_{1\beta,RA})^{-1} = (2T_{1\beta,0})^{-1} + j_{\beta,RA}[\text{RA}] = W_{\beta,0} + j_{\beta,RA}[\text{RA}]. \tag{16}$$

It is convenient to introduce the quantities

$$\Delta W = W_\alpha - W_\beta = W_{\alpha,0} - W_{\beta,0} + (j_{\alpha,RA} - j_{\beta,RA})[\text{RA}], \tag{17}$$



$$\Delta W_0 = W_{\alpha,0} - W_{\beta,0}, \quad (18)$$

$$\Delta j = j_{\alpha,RA} - j_{\beta,RA}, \quad (19)$$

$$B = \Delta W_0 + k(1 - 2f_\alpha). \quad (20)$$

With these definitions, expressions for the quantities  $X$ ,  $Y$  and  $Z$  diverge from those given in BHH, and

$$X - Y = B + \Delta j[RA], \quad (21)$$

$$Z = \sqrt{(X - Y)^2 + 4k^2 f_\alpha(1 - f_\alpha)} = \sqrt{(B + \Delta j[RA])^2 + 4k^2 f_\alpha(1 - f_\alpha)}. \quad (22)$$

It is useful to normalize the SR amplitudes to remove their dependence on total spin concentration,

$$A_{Nf} = \frac{A_f}{A_f + A_s} = \frac{1}{2} \left( 1 + \frac{\gamma}{\delta Z} \right), \quad (23)$$

$$A_{Ns} = \frac{A_s}{A_f + A_s} = 1 - A_{Nf}. \quad (24)$$

Combining Eqs. (8), (9), (21), and (22), the normalized fast component amplitude, Eq. (23), can be re-expressed as

$$A_{Nf} = \frac{1}{2} \left( 1 + \frac{(B + \Delta j[RA])D - 2kE}{\sqrt{(B + \Delta j[RA])^2 + 4k^2 f_\alpha(1 - f_\alpha)}} \right), \quad (25)$$

where

$$D = \frac{f_\alpha - \mathbf{r}(1 - f_\alpha)}{f_\alpha + \mathbf{r}(1 - f_\alpha)}, \quad (26)$$

$$E = \frac{(1 + \mathbf{r})f_\alpha(1 - f_\alpha)}{f_\alpha + \mathbf{r}(1 - f_\alpha)}, \quad (27)$$

$$\mathbf{r} = \frac{\rho_2 l_\beta}{\rho_1 l_\alpha}. \quad (28)$$

When exchange between the two states is in the slow limit (i.e., when  $k \approx 0$ ),  $A_{Nf}$  is simply related to the fraction of the more mobile component,  $f_\alpha$ , and  $\mathbf{r}$  by

$$A_{Nf}(f_\alpha, r) = \frac{f_\alpha}{f_\alpha + r(1 - f_\alpha)} = \frac{1}{1 + r(f_\alpha^{-1} - 1)} \quad (\text{slow exchange}), \quad (29)$$

which is simply equal to  $f_\alpha$  when  $\mathbf{r} = 1$  (i.e., assuming the same lineshape and perfect spectral overlap), as discussed in BHH.

In the ratio  $\mathbf{r}$ , the  $\rho_1$  and  $\rho_2$  parameters account for the offsets of resonance maxima relative to an arbitrary observe position, and are simply the fraction of maximum amplitude at the observe position. In practice, the observe position is at the maximum of the central resonance line, which is generally determined by the narrow resonance of the more mobile component (state  $\alpha$ ) and so that  $\rho_1 = 1$ . The

offset of the  $\beta$  resonance from this position is determined by differences in  $g$  factor, and is small at X-band; under any condition the relatively broad resonance of the immobilized  $\beta$  spins justifies the assumption that  $\rho_2 \approx 1$ , and hence  $\mathbf{r} \approx l_\beta/l_\alpha$  with little error. In any case, values for  $\rho_1$  and  $\rho_2$  can be directly determined from spectral simulations and/or field-swept SR-detected (FSRD) absorption spectra, as discussed further below. For generality, the  $\rho$  factors are retained in the expressions.

### 3.2 The [RA]-Dependence of $A_{Nf}$ in Systems of Intermediate Exchange

The normalized SR amplitude of the fast relaxing component,  $A_{Nf}$ , depends in general on the RA concentration. The nature of this dependence is revealed in the first derivative of  $A_{Nf}$  with respect to the concentration of RA,

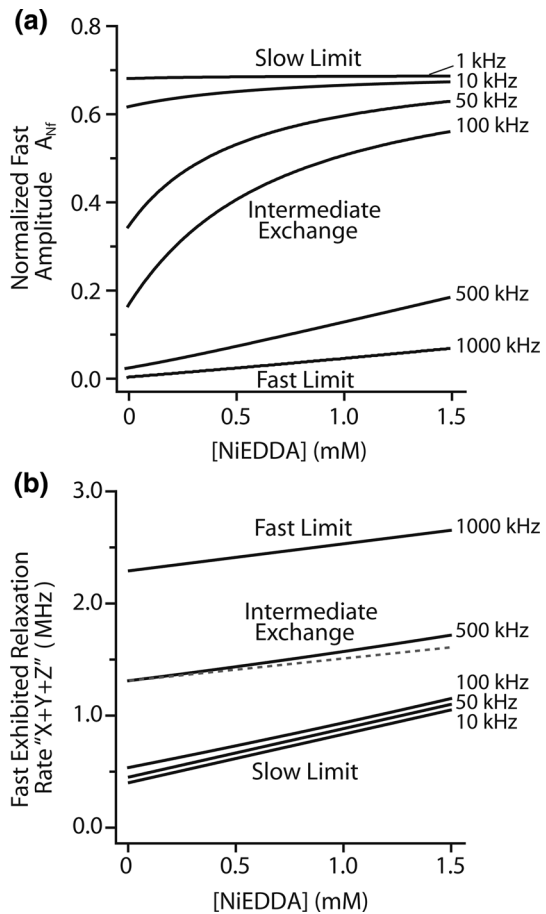
$$\frac{dA_{Nf}}{d[\text{RA}]} = A'_{Nf} = (k\Delta j) \left[ \frac{2kDf_\alpha(1-f_\alpha) + E(B + \Delta j[\text{RA}])}{\left( (B + \Delta j[\text{RA}])^2 + 4k^2f_\alpha(1-f_\alpha) \right)^{3/2}} \right]. \quad (30)$$

Apparent from Eq. (30) is the fact that normalized SR amplitudes of spin-labeled protein samples are affected by the relaxation agent concentration only in select cases. For example, in the slow exchange limit (i.e., as  $k \rightarrow 0$ )  $A'_{Nf} \rightarrow 0$  and the pre-exponential amplitudes of a slow exchange system are independent of relaxation agents such as Nickel (II) EDDA (“NiEDDA”) or oxygen. The derivative  $A'_{Nf}$  is also zero when there is no differential accessibility between the two states of the nitroxide (i.e., whenever  $\Delta j = 0$ ). However, it has been shown for a large database that R1 mobility and accessibility are directly correlated, i.e., an immobilized nitroxide is less accessible than one with high mobility [28, 29]. Therefore, for cases where SR is suited to study exchange, i.e., where the nitroxide is in exchange between states of relatively high and low mobility, it is likely that  $\Delta j \neq 0$ .

In intermediate exchange and for  $\Delta j > 0$ ,  $A'_{Nf}$  is always positive. At high concentrations of RA, the slope  $A'_{Nf}$  approaches zero, and the normalized amplitude approaches the value expected for the slow exchange limit. The RA concentration-dependent behavior of  $A_{Nf}$  for various exchange rates is illustrated in Fig. 4a, and provides a simple and robust test for intermediate exchange in two-component systems: if  $A_{Nf}$  is invariant to the addition of a relaxation agent, the system is in the slow exchange limit, otherwise, its exchange lifetime lies in the ‘intermediate regime’ with an approximate dynamic range of 1–100  $\mu\text{s}$  (Fig. 4a). A particular feature of the plot is that the normalized amplitude of the fast relaxing component is under-represented compared to the analytical concentration of spin in that component.

For comparison, Fig. 4b shows the dependence of the relaxation rate for the fast relaxing component ( $W_f = X + Y + Z$ , Eq. (5)) on RA concentration. Unlike the trend for  $A_{Nf}$ , the rates always depend on RA concentration. In the slow exchange limit, the dependence on RA concentration is strictly linear with a slope equal to the accessibility  $j_f$ . Although there is a relatively strong variation in  $W_f$  with  $k$  in the range of 50–500 kHz at any RA concentration, such variation is of little use in identifying intermediate exchange without prior knowledge of the intrinsic  $T_1$ s of

**Fig. 4** Simulated relaxation rates illustrating the dependence of normalized fast amplitudes and relaxation rates on RA concentration, as a function of exchange rate constant,  $k$ . **a** The dependence of  $A_{NF}$  on RA concentration according to Eq. (25). **b** The dependence of the experimental fast relaxation rate constant,  $X + Y + Z$ , on RA concentration as predicted by Eqs. (11)–(28). For these simulated data, the following parameters were used:  $T_{1\alpha,0} = 2.4 \mu\text{s}$ ,  $T_{1\beta,0} = 3.9 \mu\text{s}$ ,  $j_x = 0.22 \text{ MHz/mM}$ ,  $j_\beta = 0.00 \text{ MHz/mM}$ ,  $f_x = 0.60$ ,  $r = 0.72$ . The exchange rate  $k$  was varied from 1 to 1000 kHz as indicated on the right, which corresponds to exchange lifetimes in the range of 1  $\mu\text{s}$ –1 ms. The *straight dotted line* in **b** is shown to emphasize the slight curvature of the trends in the intermediate exchange regime



the components (i.e., in the absence of exchange and added RA). It is worth noting that in some cases reasonable estimates of the intrinsic  $T_1$ s can be made from nitroxide mobility determined from simulations, and an estimate of  $k$  can be made from these data and experimental values of  $W_f$  [12]. However, the presence of intermediate exchange can only be rigorously discerned by the nonlinearity of the plot [12], which is weak as indicated by the straight dotted line for the case for 500 kHz exchange rate. This small deviation from linearity makes its detection in experimental data challenging, therefore rate analysis alone is often insufficient for the identification and quantification of intermediate exchange.

### 3.3 $T_1$ -Based Spectral Editing in the Slow Exchange Limit

In the slow exchange limit, the amplitude of relaxation for a given  $T_1$  in a bi-exponential relaxation curve is simply related to the population of spins with that  $T_1$ . If SR data is collected as a function of magnetic field across the spectrum, the individual amplitudes will provide the contribution of each component to the

spectrum. Thus, if the  $T_1$ s for the two states are sufficiently different, individual contributions to the CW spectrum from the two components can be deduced at each field and the individual spectral lineshapes resolved. One example of this FSRD spectral editing is illustrated in Sect. 5.2.

## 4 Experimental Methods

### 4.1 Preparation of Spin-Labeled Proteins

#### 4.1.1 T4 Lysozyme 118R1, 130R1, 131R1, and 121A/133A/130R1

The pseudo-wild-type T4L construct (pHSe5) containing the substitutions C54T and C97A was a generous gift from F.W. Dahlquist (University of California, Santa Barbara, CA). Preparations of the mutants of T4 Lysozyme (T4L) and the protein purifications have been previously reported [9, 30–32]. Spin labeling was conducted for 30 min at room temperature at tenfold molar excess of (1-oxy-2,2,5,5-tetramethylpyrrolinyl-3-methyl)-methanethiosulfonate (a gift of Kalman Hideg, University of Pecs, Hungary) in buffer (50 mM MOPS, 25 mM NaCl at pH 6.8). Excess spin-label reagent was removed using a HiTrap desalting column (GE Healthcare) and the protein was concentrated using Amicon Ultra 10,000 MWCO (Millipore).

#### 4.1.2 Apo-rI-FABP 75R1

The wild-type rat intestinal fatty acid binding protein in plasmid pET11d (Novagen, Madison, WI) was a generous gift from Alan K. Kleinfeld (Torrey Pines Institute for Molecular Studies, San Diego, CA). The preparation, expression, purification, and spin labeling of the 75C mutant have been previously reported [33].

### 4.2 CW and Saturation Recovery

#### 4.2.1 General

All samples were prepared such that their final spin-labeled protein concentration was between 250 and 500  $\mu$ M. To slow rotational diffusion of the protein, samples contained 30% w/w sucrose. Nickel (II) EDDA was synthesized according to [34]. All sample spectra were recorded in a nitrogen atmosphere at a controlled temperature of 298 K. Samples (3–6  $\mu$ l) were loaded into a gas-permeable TPX capillary (methylpentene polymer, inner diameter of 0.6 mm, Molecular Specialties Inc., Milwaukee, WI, USA). Temperature and atmosphere around the sample during measurement were controlled by the commercial Bruker temperature control unit, which employs nitrogen flow from a liquid nitrogen boiler and heater apparatus. All samples were equilibrated with a nitrogen atmosphere for at least 15 min to ensure no relaxation effects due to the presence of ambient oxygen.

### 4.2.2 CW EPR

CW EPR spectra were recorded at X-band on a Bruker E-580 spectrometer fitted with a two-loop one-gap resonator (Medical Advances, Milwaukee, WI, USA) over a field range of 100 G, at 2.0 mW incident power, a modulation frequency of 100 kHz, and a modulation amplitude of 1 G [35]. Note that none of the NiEDDA-containing samples exhibited exchange broadening effects detected by CW EPR in the concentration range of 0–1.5 mM.

### 4.2.3 SR EPR

SR data were collected on a Bruker E580 spectrometer fitted with a Stanford Research Instruments amplifier (Part #SR445A) in place of the video amplifier originally supplied with the spectrometer. Data acquisition was under the control of Bruker-supplied software, and selection of parameters for the long-pulse experiments followed the general guidelines provided by Hyde [36, 37]. In all SR experiments, a 250 mW pump pulse provided by the electron–electron double resonance (ELDOR) source was used. For all mutants, a 4  $\mu$ s pump pulse was used to ensure complete saturation of both spectral components. A 200  $\mu$ W CW observe power was used with detection set to the same frequency as the pump pulse. This observing power is sufficiently high to shorten the relaxation times, but this does not influence the amplitude ratios or global fitting of the SR data to determine exchange rates; higher observe power does significantly reduce data acquisitions times [24–26]. For experiments other than FSRD both the excitation and detection were performed at the maximum absorbance of the  $m_I = 0$  hyperfine line of the  $^{14}\text{N}$  nitroxide spectrum, and the total number of accumulations of each measurement was 2.10 million over the course of approximately 6 min; each measurement was independently made three times and signal-to-noise for the individual traces ranged from 120 to 415 for the different mutants studied. For each mutant at each NiEDDA concentration, the average trace of the three replicate curves obtained was used in analysis described below.

Each SR curve was acquired as 2048 points at 50 MHz, with an analog bandwidth of 20 MHz. Typically 131,072 accumulations were acquired on- and off-resonance using a 1 Hz field step of 40 G downfield. All SR spectra were phase-corrected prior to analysis, and the first 238–260 data points (out of 2048), depending on the sample, were trimmed from the relaxation curves, as these regions of the spectra included remnants of the instrumental defense pulse at the apparent  $t = 0$  (Fig. 2). The “true time zero” of the relaxation curve was determined from the amount of trimmed data and known pulse timing sequence, i.e., lengths and positions of saturating and defense pulses (Fig. 2). For the Bruker E580 and loop-gap resonator combination used, this time was 280 ns immediately prior to the end of the defense pulse, which was verified via the system’s transmission monitor (“TM”). All SR data and UPEN analyses presented herein were corrected for this true time zero.

### 4.3 Simulation of CW EPR Spectra to Determine the Fractional Populations

To determine equilibrium populations from two-component CW spectra, they were fit using the microscopic order–macroscopic disorder (MOMD) model of Freed and co-workers [38]. Starting values for the elements of the A and g magnetic tensors for solvent-exposed sites were  $A_{xx} = 6$  G,  $A_{yy} = 6$  G,  $A_{zz} = 37$  G,  $g_{xx} = 2.0078$ ,  $g_{yy} = 2.0055$ ,  $g_{zz} = 2.0023$ ; for buried and solvent-inaccessible sites,  $A_{xx} = 5$  G,  $A_{yy} = 4.6$  G,  $A_{zz} = 35.5$  G,  $g_{xx} = 2.0082$ ,  $g_{yy} = 2.0065$ ,  $g_{zz} = 2.0023$  [39]. The fitting procedure is described in detail elsewhere [40]. Absorption lineshapes of the separate components from the simulated fits (as shown in Figs. 2, 3b) were obtained by direct integration of the CW spectra and the second integrals obtained to determine the fractional populations of each component ( $f_\alpha$ ,  $f_\beta$ ) using the data analysis software Origin (version 7.5, OriginLab, Northampton, MA).

### 4.4 Analysis of SR Relaxation Curves to Determine Amplitudes and Exchange Rates

#### 4.4.1 Determination of Normalized Fast Component Amplitudes ( $A_{Nf}$ )

Averaged SR curves for each mutant at each NiEDDA concentration were fit via the UPEN method [19, 20] using a LabVIEW program written in-house (available upon request) that produces a relaxation time distribution of the form,

$$i_{SR} = 1 - \sum_i w_i \exp(-t/T_{1i}) + y_0, \quad (31)$$

where  $y_0$  is a linear offset proportional to the system's z-magnetization at equilibrium [25], and  $T_{1i}$  spans 0.5–15.5  $\mu$ s, divided into 256 points, with  $w_i$  as a weighting coefficient. Included in the UPEN analysis model are amplitude, slope, and curvature penalties added to the squared fitting error of Eq. (31), the total of which is minimized in the SR data fit; for more details regarding the method and underlying theory, refer to References [19, 20]. The resulting relaxation time constant distributions from all UPEN analyses of data were bimodal with two peaks corresponding to the fast and slow relaxing states of each mutant studied. Relative peak areas, and thus  $A_{Nf}$  and  $A_{Ns}$  values, were obtained via numerical integration and normalization of the UPEN analysis output and are directly proportional to the relaxation amplitude of the corresponding component.

#### 4.4.2 Global Fits of UPEN-Analyzed SR Data to Estimate Exchange Rates

For cases of intermediate exchange, identified by curvature of the  $A_{Nf}$  vs [NiEDDA] plot, the exponential relaxation rates and amplitudes are both functions of NiEDDA concentration, and these values are determined quantitatively from the  $T_1$  distributions produced by UPEN analysis;  $A_{Nf}$  is determined as the fractional area of the fast relaxing population, and in the context of the two-site exchange model, the median peak positions of the UPEN distributions are taken as the relaxation time

**Fig. 5** Ribbon diagrams of the proteins, locations of spin-labeled sites and CW EPR spectra. Spheres at  $C_\alpha$  atoms identify the spin-labeled sites in the indicated protein. In each case, the experimental spectrum (black, upper trace) and corresponding simulation (red, lower trace) from which  $\mathbf{r}$  and  $f_z$  values were estimated are shown. For T4L 118R1, the spectrum has been corrected by removal of a small contribution of free spin label (<1%), which forms due to dissociation of the R1 side chain from the protein (color figure online)

constants  $(X + Y + Z)^{-1}$  and  $(X + Y - Z)^{-1}$  (Eq. (5)). The amplitudes and time constants are each functions of the parameters  $T_{1\alpha,0}$ ,  $T_{1\beta,0}$ ,  $j_\alpha$ ,  $j_\beta$ ,  $k$ ,  $f_z$ , and  $\mathbf{r}$ , all of which are expected to be independent of NiEDDA concentration. To estimate exchange rate constants, the set of amplitudes and time constants obtained from UPEN analysis for the six NiEDDA concentrations were fit globally by least squares to this set of shared variables, using the functional dependence of amplitudes and rates given by Eqs. (11), (12), (15)–(27). To reduce the number of variable fitting parameters,  $f_z$  and  $\mathbf{r}$  were determined independently from CW lineshape analysis. The global analysis was performed using a LabVIEW program (written in-house, available upon request).

#### 4.4.3 Field-Swept SR-Detected (FSRD) Spectra for Systems in Slow Exchange

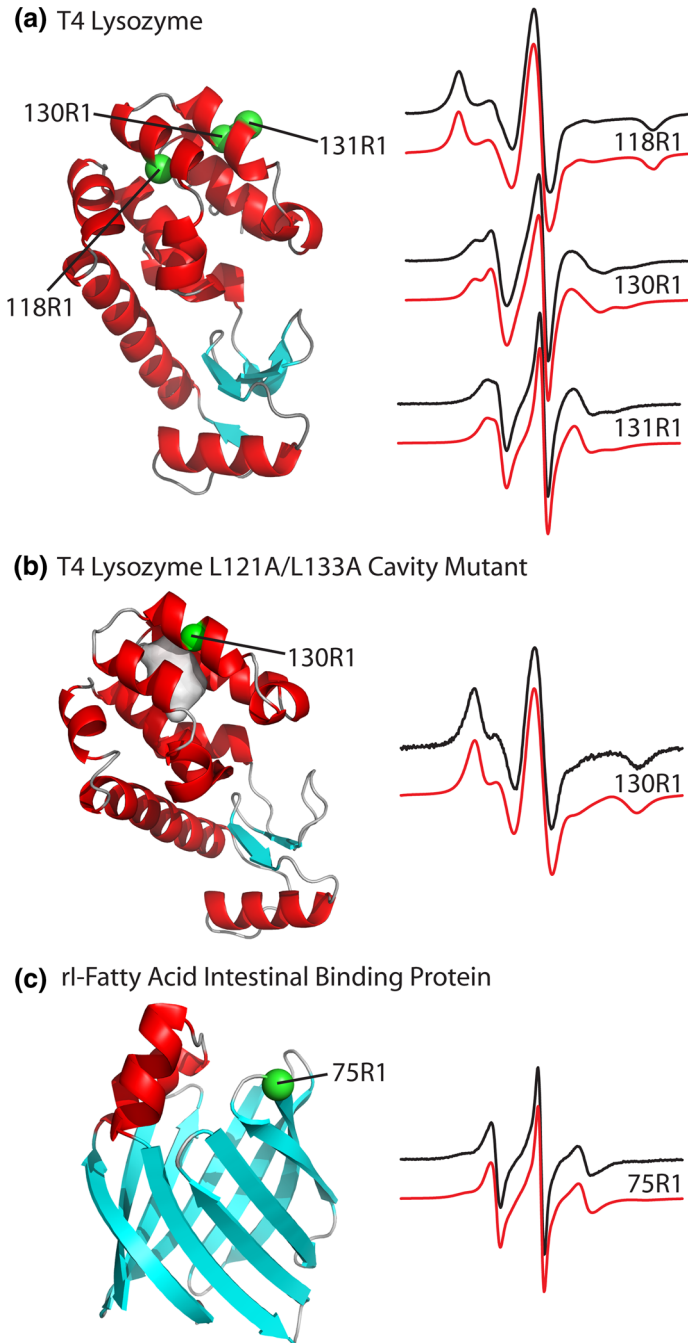
For the FSRD experiment, relaxation curves were acquired for Mixture B ([NiEDDA] = 0 mM) at 30 different field positions within the  $m_I = 0$  resonance line. The total number of accumulations at a given field position in the spectrum was 1.05 million over the course of approximately 3 min. For slow exchange, the relaxation amplitudes are simply proportional to populations and independent of exchange, and the entire set of relaxation curves were globally fit with least squares to the bi-exponential function,

$$A = A_f e^{-(t/T_{1f})} + A_s e^{-(t/T_{1s})} + A_0, \quad (32)$$

with parameters  $A_f$ ,  $A_s$ , and  $A_0$  unconstrained, but with  $T_{1f}$  and  $T_{1s}$  shared for all data sets (as the relaxation time constants should not vary with field within a single spin manifold). The output of the absolute field-dependent amplitudes is plotted as a function of field to obtain the FSRD spectrum. All relative errors in amplitude determination from these fits (as 95% confidence intervals) were <5%.

## 5 Results

To verify the validity of Eq. (25) for the relationship between normalized fast component amplitude and RA concentration, and to demonstrate the utility of the result, SR data were obtained for spin-labeled mutants of T4 Lysozyme (T4L 118R1, 130R1, 130R1/121A/133A and 131R1) and rat intestinal Fatty Acid Binding Protein (FABP 75R1) (Fig. 5). Except for T4L 131R1 and 130R1/121A/133A, the mutants were selected to represent two-site exchange; each has two components in both the CW spectrum and the saturation recovery signal, indicating intermediate or slow exchange on the  $T_1$  timescale.



The CW spectra of T4L 131R1 and 130R1/121A/133A are each single component; that for 131R1 reflects the rapid anisotropic motion typical of R1 at a solvent-exposed helical surface site (Fig. 5a) [40], while that for L121A/L133A/



130R1 is characteristic of a buried and strongly immobilized site (Fig. 5b). The mutations L121A/L133A create a cavity in the T4L molecule (shaded gray, Fig. 5b), and earlier work has shown that 130R1 in the background of this mutant moves into the empty cavity where it is completely buried and immobilized [32]. Mixtures of these two spin-labeled T4L mutants were prepared to mimic the behavior of a non-exchanging two-component system, each with a known population, markedly different mobility (and hence different  $T_1$ ), and different RA accessibility.

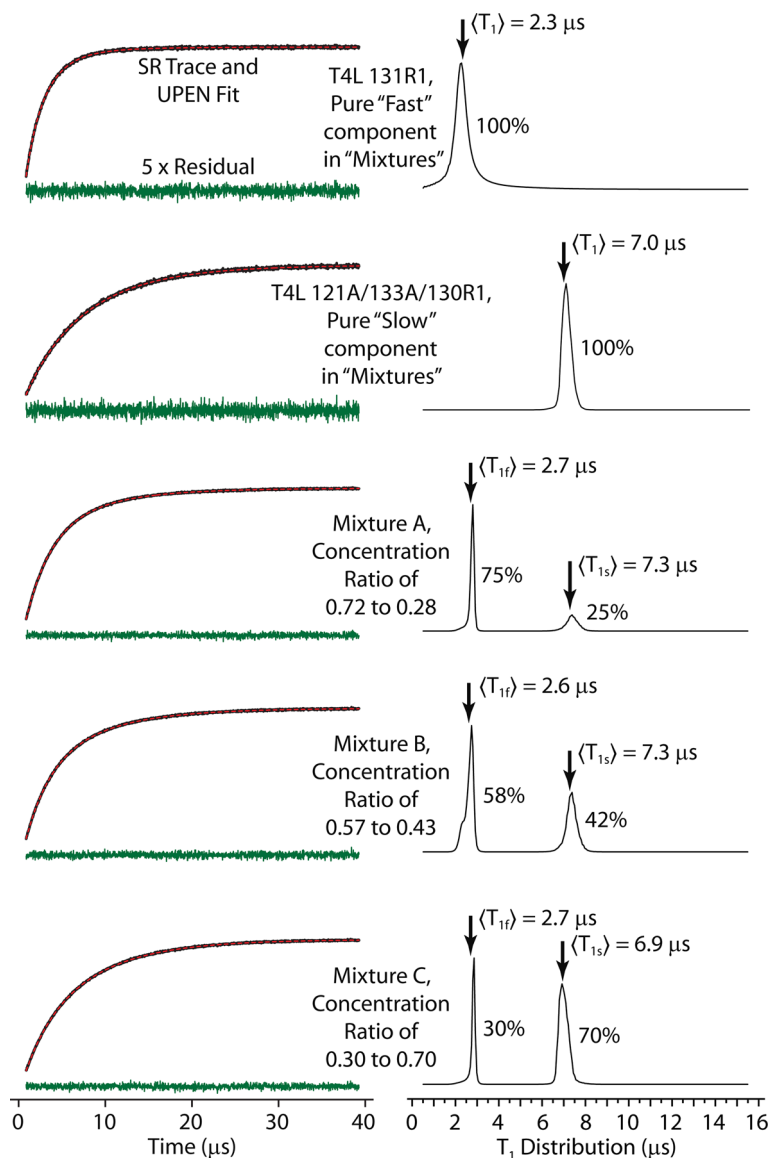
In the following sections, the above mutants are employed to illustrate the use of SR recovery amplitude information for identification and analysis of intermediate exchange on the  $T_1$  timescale and in spectral editing for systems in slow exchange.

### 5.1 The [NiEDDA]-Dependence of $A_{Nf}$ for Slow and Intermediate Exchange Systems

The normalized fast amplitude,  $A_{Nf}$ , of a spin-labeled protein system is dependent on the RA concentration present as well as the exchange regime (Eq. (25)). In particular,  $A_{Nf}$  is predicted to increase with increasing RA concentration for intermediate exchange lifetimes ( $\sim 1$ – $100 \mu\text{s}$ ), and is independent of RA concentration in the slow exchange limit (Fig. 4a).

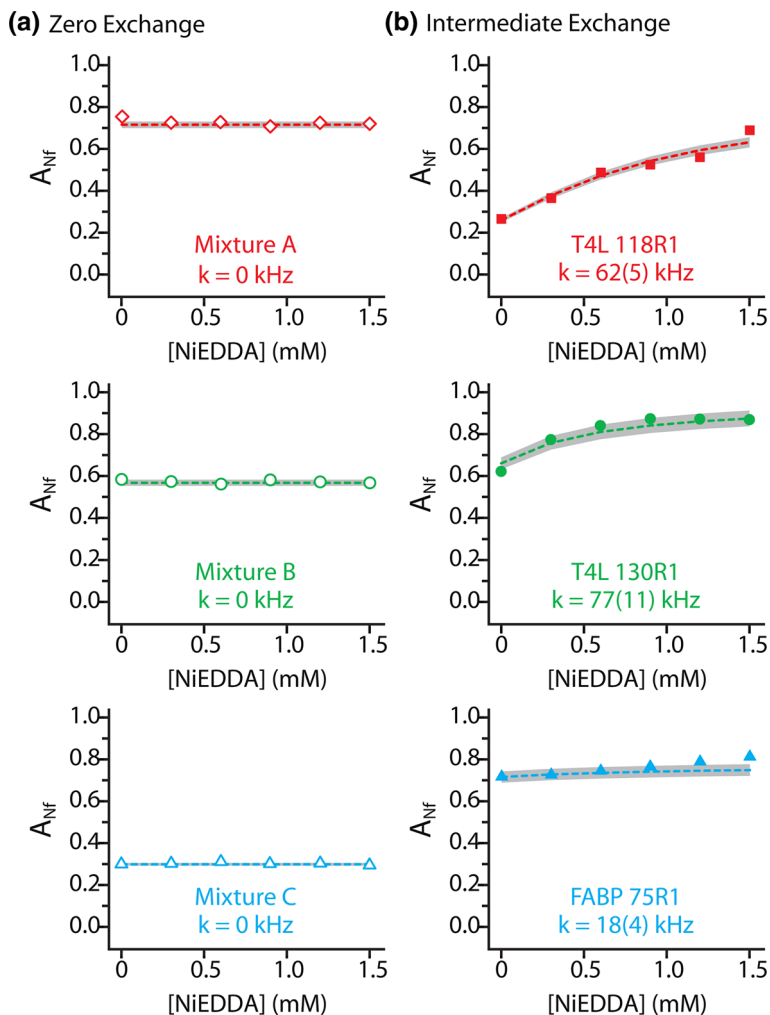
To test these predictions,  $A_{Nf}$  was experimentally determined from relative peak areas in UPEN analyses of SR curves as a function of NiEDDA concentration for systems known to be in the slow and intermediate exchange regimes. To represent a slow exchange limit sample set, three different mixtures (*A*, *B*, *C*) of T4L 131R1 and T4L 130R1/121A/133A were employed. The analytical concentration ratio of spins (131R1):(130R1/121A/133A) for each mixture was determined by fitting the CW EPR spectrum of the mixture to weighted amounts of the individual spectra and found to be for *A* 0.72:0.28; *B* 0.57:0.43; *C* 0.30:0.70. Figure 6 shows the zero-NiEDDA SR traces and UPEN fits for these single mutants and three prepared mixtures. Fits to the SR data and the resulting  $5 \times$  residuals (left) show the high quality of fit characteristic of the UPEN method; the UPEN relaxation time distribution plots (right) confirm that the three mixtures have behaviors that are combinations of those of the two single-dynamic state mutants. Relative peak areas from the UPEN distribution plots yielded  $A_{Nf}$  and  $A_{Ns} = 1 - A_{Nf}$  for each mixture and the values are essentially identical to the spin concentration ratio of the components as indicated in the figure. Arrows on the UPEN traces indicate the position of the median  $T_1$ s for each population, and comparison of these values with bi-exponential fits to the same SR data gave excellent agreement ( $\leq 0.2 \mu\text{s}$  deviation).

Figure 7a shows that  $A_{Nf}$  values for these mixtures are indeed independent of NiEDDA concentration, verifying the prediction from Eq. (30) when  $k = 0$ . For these samples the expected values of  $A_{Nf}$  can be calculated using Eq. (29) with the estimated  $f_x$  and  $\mathbf{r}$  values as determined from the simulated spectrum (Fig. 3). For Mixture A this gives  $A_{Nf} = 0.72$ , which agrees with the experimental value of 0.72 from UPEN analysis. Likewise, for Mixture B the calculated and measured values of  $A_{Nf}$  are 0.57 and 0.58, respectively, and in Mixture C the  $A_{Nf}$  values are 0.30 and 0.31, respectively.



**Fig. 6** UPEN analysis of SR data for T4L 131R1, T4L 121A/133A/130R1, and “zero-exchange” mixtures in the absence of NiEDDA. *Left* SR data (black traces), UPEN fits (red dashed lines), and 5× residuals (green traces) for the two single state mutants and three non-exchanging protein mixtures studied. *Right* UPEN fits output as  $T_1$  relaxation time distribution plots, where vertical arrows indicate average  $T_1$  for each state calculated from peak area, and relative peak areas for the mixtures indicated were calculated by integration (color figure online)

To explore the dependence of  $A_{Nf}$  on RA concentration for intermediate exchange, we selected three spin-labeled mutants for which evidence exists that the two observed EPR spectral components arise from conformational exchange. These



**Fig. 7** Experimental dependence of  $A_{Nf}$  on NiEDDA concentration for spin-labeled proteins. **a** zero and **b** intermediate exchange regimes. Data points plotted are from integration of peak areas obtained via UPEN analysis of individual [NiEDDA]-dependent SR curves, while the *dashed lines* indicate fits of these points to the global exchange model (Eqs. (5), (23), (25)). Gray shading around the *dashed lines* denotes errors in the global fits, propagated from fitting parameter errors, given in Table 1. Zero slope for  $A_{Nf}$  with respect to NiEDDA concentration is expected for systems of zero exchange, whereas a positive curvature indicates intermediate exchange (lifetimes 1–100  $\mu$ s)

proteins are T4L 118R1, T4L 130R1, and FABP 75R1. Spin-labeled site 118 in T4 Lysozyme is categorized as a buried site; the nitroxide side chain has been found to over-pack the hydrophobic core and destabilize the F helix of the protein [31]. As such, the two-component CW EPR spectrum is believed to be the result of exchange between the folded and unfolded states of the short F helix (Fig. 5a) [30]. If the lifetime of Helix F conformational exchange is on the order of  $\sim 1$ –100  $\mu$ s, then  $A_{Nf}$  should exhibit a positive dependence on NiEDDA concentration. Figure 7b (left

panel, top) shows that the normalized fast amplitude for this mutant is strongly dependent on NiEDDA concentration, and thus we conclude its exchange to be in the intermediate regime. In this case of intermediate exchange and of those below,  $A_{Nf}$  is not simply related to  $f_z$  and  $\mathbf{r}$ , but also depends on the exchange rate (Eq. (25)).

Residue 130R1 resides at a contact site between helices in native T4L (Fig. 5a). The crystal structure at 100 K shows a single rotamer of R1 but the CW spectrum in solution has two well-resolved components [41]. BHH investigated T4L 130R1 with SR and concluded that the residue was in intermediate exchange based on a bi-exponential recovery and a slight curvature in plots of the relaxation rates ( $W_\alpha$ ,  $W_\beta$ ) vs. [NiEDDA]. As predicted for a system in intermediate exchange,  $A_{Nf}$  for T4L 130R1 is dependent on NiEDDA concentration with a positive slope (Fig. 7b center panel).

Residue 75R1 in FABP is in a turn between  $\beta$  strands that cover a putative portal to the ligand binding site (Fig. 5c). NMR relaxation studies have verified conformational exchange in this region [42], and the CW EPR spectrum has two components that are modulated by osmotic perturbation, consistent with conformational exchange [33]. Here,  $A_{Nf}$  is a weakly increasing function of NiEDDA concentration, indicative of exchange in the intermediate range (Fig. 7b, bottom panel, right hand column).

Collectively, the above results are consistent with predictions of Eq. (25), and reveal the nonlinearity of  $A_{Nf}$  with NiEDDA concentration, thus identifying intermediate exchange.

## 5.2 Spectral Editing with Field-Swept Saturation Recovery in the Slow Exchange Limit

Figure 8a shows the experimental CW spectrum of Mixture B containing spin concentration ratios for [T4L131R1:130R1/121A/133A] of [0.57: 0.43] (black trace), and the individual components (red and green traces, respectively) that make up the mixture; an expanded view of the center line, indicated as a rectangle in Fig. 8a, is shown in Fig. 8b. The differing alignments of the spectra with respect to magnetic field are attributed to the different effective g-tensors of the nitroxides in the two environments. Field-swept saturation recovery EPR data were collected at

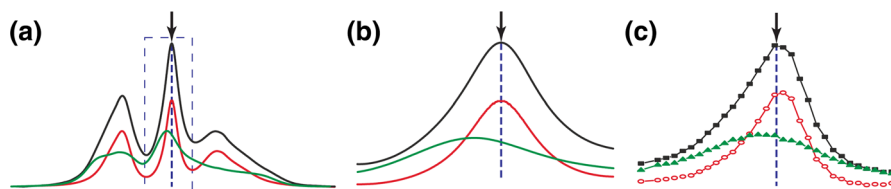


**Fig. 8** Integrated-CW and FSRD absorption EPR spectra for a mixture of T4L 131R1 and L121A/L133A/130R1. **a** The simulated spectrum of Mixture B together with the individual spectral components obtained from the simulation. **b** Expanded boxed region around center line from **a**. **c** The FSRD absorption spectrum. The arrows and dashed lines mark the position of the pump and observer microwave sources (color figure online)

30 field points across the width of the center line and Fig. 8c shows the resulting FSRD absorption spectra for the individual components and their sum as determined from the corresponding amplitudes of the fast and slow relaxing components. As is evident, there is excellent agreement with the FSRD and CW spectra. The value of the offset parameters ( $\rho$ ) can be directly determined from the FSRD spectra without recourse to CW-spectral simulations, and in this case, they are clearly in good agreement. The observer field position (arrow) is essentially that of the sharp mobile component, so the offset parameter  $\rho_1 = 1$  by definition. Due to the breadth of the immobile component, assuming that  $\rho_2 \approx 1$  results in only a small error ( $\rho_2$  appears to be  $>0.95$ ). In principle, entire spectral lineshapes can be determined from a wide field scan and the relative populations of the components ( $f_x$ ) determined from direct integration, but this is a time-consuming exercise.

### 5.3 Estimation of Exchange Rate Constants

Based on the data in Fig. 7 and other studies, T4L 118R1, T4L 130R1, and FABP 75R1 exhibit intermediate exchange. To extract exchange rate constants,  $A_{Nf}$  and relaxation rate information from the UPEN analysis of SR data collected at multiple NiEDDA concentrations were fit globally as discussed in the Experimental section to obtain values for  $T_{1\alpha,0}$ ,  $T_{1\beta,0}$ ,  $j_x$ ,  $j_\beta$ , and  $k$ .

In BHH, SR data were fit to Eq. (5) using rate data alone. While this was sufficient to distinguish fast from slow and intermediate exchange, only in ideal cases estimated numerical values for the exchange rate constant,  $k$ , could be derived. Despite having high quality SR data at many different RA concentrations, fitting only relaxation time constants to the model presented in BHH proved to be problematic due to correlations between parameters and the resulting large uncertainties; for many cases convergence could not be reached in the fitting process. Because the amplitudes and rates have a different functional dependence on the above listed parameters, a global fit of the UPEN analyses—including rates (from peak positions) and amplitudes (from relative peak areas)—for a set of experimental SR curves obtained at different NiEDDA concentrations provided significantly reduced relative errors in the results.

Figure 9 shows the SR data obtained for T4L 118R1, T4L 130R1, and FABP 75R1 at multiple NiEDDA concentrations (black traces) along with the fits from UPEN analysis (red dashed lines), with excellent agreement between the two. Inset in each plot are the UPEN distributions (black traces) obtained from fitting the SR data. From the UPEN fits, a set of  $A_{Nf}$  and relaxation rate values are obtained. This set was globally fit to the two-site exchange model as described in the Sect. 4. Table 1 provides the parameters obtained from the global fits to the three zero- and three intermediate-exchange samples. The  $A_{Nf}$  values computed from these global fit parameters are plotted as a function of [NiEDDA] (Eq. (25)) and shown in Fig. 7 as dashed lines, within gray bands that encompass the range of estimated error. The largest relative error in estimated exchange rate constant seen is for FABP 75R1 ( $\sim 20\%$ ), where the exchange rate constant (17 kHz) is closest to the slow limit for detection by the SR method ( $\approx 10$  kHz) (Fig. 4a); hence the small slope of the  $A_{Nf}$  vs NiEDDA concentration plot of Fig. 7b (right panel).

**Fig. 9** [NiEDDA]-dependent SR relaxation data and UPEN fits for the three mutants in the intermediate exchange regime. **a** T4L 118R1, **b** T4L 130R1, and **c** FABP 75R1. SR data (*black recovery curves*) were analyzed by the UPEN method (fits plotted as *red dashed lines*) yielding the  $T_1$  distributions plotted in the *inset*. For each set of stacked traces (SR and UPEN) [NiEDDA] = 0.0, 0.3, 0.6, 0.9, 1.2, and 1.5  $\mu\text{M}$ , *bottom to top* (color figure online)

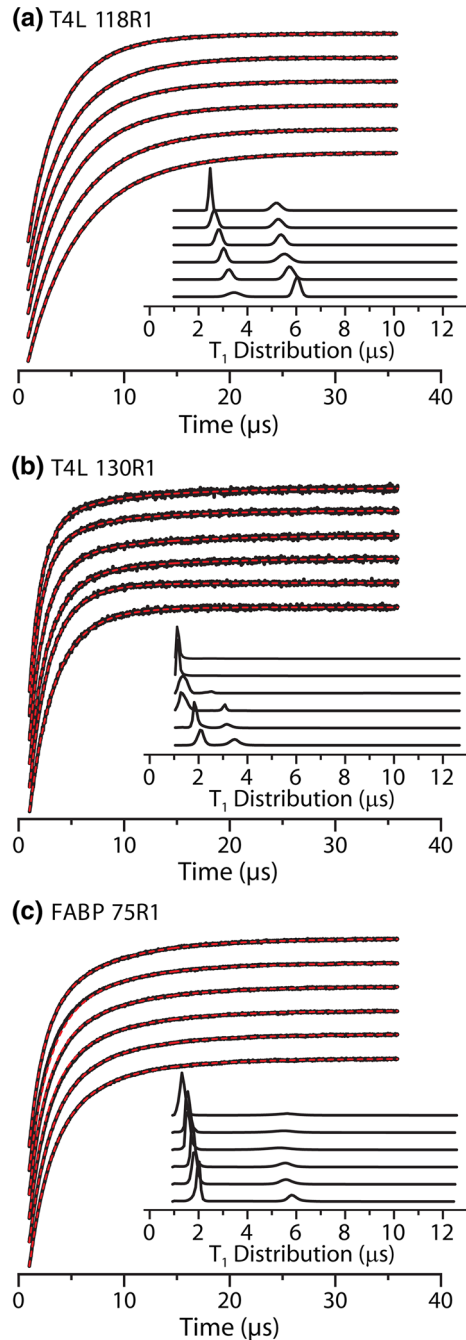


**Table 1** Determined parameters from global fits of [NiEDDA]-dependent SR curves via UPEN analysis for multiple spin-labeled protein mutants. Numbers in parentheses represent standard deviations of fitting parameters

Mutant <sup>a</sup>	$T_{1\alpha,0}$ ( $\mu$ s)	$T_{1\beta,0}$ ( $\mu$ s)	$j_{\alpha,\text{Ni}}$ (kHz/mM)	$j_{\beta,\text{Ni}}$ (kHz/mM)	$k$ (kHz)	$f_{\alpha}$ <sup>b</sup>	$r$ <sup>c</sup>
Mixture A	2.8 (0.1)	7.2 (0.5)	100 (5)	1 (5)	0 (0)	0.61	0.62
Mixture B	2.6 (0.1)	7.3 (0.6)	95 (6)	2 (6)	0 (1)	0.45	0.62
Mixture C	2.9 (0.1)	7.1 (0.4)	100 (5)	0 (5)	0 (2)	0.21	0.62
T4L 118R1	4.7 (0.2)	9.5 (1.3)	51 (6)	0 (6)	62 (5)	0.80	0.77
T4L 130R1	2.4 (0.1)	5.3 (1.0)	173 (14)	51 (14)	77 (11)	0.84	0.29
FABP 75R1	2.2 (0.1)	6.1 (0.7)	122 (10)	2 (10)	18 (4)	0.59	0.43

<sup>a</sup> All samples were studied by SR in triplicate in the presence of six different Nickel (II) EDDA concentrations ranging from 0 to 1.5 mM

<sup>b</sup> Relative fraction of state “ $\alpha$ ”, the more mobile component; determined by spectral simulation and fixed in these global fits

<sup>c</sup> The ratio “ $r$ ”, defined by Eq. (28) and discussed in the text; determined by spectral simulation and fixed in these global fits

The values obtained from fitting for  $T_{1\alpha,0}$  and  $T_{1\beta,0}$  are within the expected range for the correlation time of the corresponding nitroxide [12], and the accessibilities are also as expected, i.e.,  $\approx 0$ , for buried nitroxides of low mobility and high for solvent exposed sites.

## 6 Discussion

The experimental identification of equilibrium conformational exchange in proteins and determination of the relevant equilibrium constants and exchange rates is central to elucidating mechanisms of protein function. The method of SDSL-EPR has distinct advantages of timescale and sensitivity for these purposes [8]. Earlier work has shown that two-component EPR spectra in proteins containing R1 can arise either from R1 rotamer exchange [31] or from protein conformational equilibria. It was further shown that osmotic perturbation [11, 33] and high pressure [43] EPR can distinguish these possibilities under certain conditions. Perhaps the most general strategy for this purpose was found to be SR, which revealed that R1 rotamer exchange was in the fast limit, giving a single exponential recovery despite a two-component CW EPR lineshape, while conformational exchange had a bi-exponential recovery [12]. Thus, a combination of the above methods can identify equilibrium conformational exchange with reasonable certainty, and spectral simulations can provide the populations of states and hence the equilibrium constants and free energy differences. The remaining challenge for SDSL-EPR is to determine the timescale for such exchange events, and addressing this challenge with SR-EPR is the main subject of this report.

To date, SR data for nitroxides in spin-labeled proteins have been analyzed only in terms of relaxation rates, and for the determination of Heisenberg exchange and solvent accessibility [44, 45]. For distinguishing fast from slow and intermediate

exchange [12], rate data alone are adequate. However, the work of BHH and the results presented above (Fig. 4b and discussion thereof) make it clear that rate data alone are not sufficient for quantitative determination of exchange rates in the window of 10 kHz–1 MHz available to the SR method. This situation motivated the present study to include relaxation amplitudes together with rates in a global analysis of SR data. Quantitative determination of experimental SR amplitudes is more demanding than that for rates, and requires a definition of the true  $t = 0$  for the recovery curve, complete saturation of all spectral components with a pulse long compared to spectral diffusion processes, and knowledge of the central lineshape features of the spectra. As discussed below, this latter requirement introduces the most uncertainty in determination of exchange rates by the SR methods.

An interesting outcome of the analysis presented here is that the exponential relaxation amplitudes are not directly related to the equilibrium populations of the states observed in the CW EPR spectra except in the case of slow exchange ( $k < 10$  kHz), and this criterion cannot be judged from the EPR spectra alone without SR data. In situations where slow exchange is confirmed by SR, the equilibrium populations can be extracted from the recovery amplitudes given values of the lineshape parameter  $\mathbf{r}$ . For the methods presented here, this could be considered redundant information because  $\mathbf{r}$  can be estimated from spectral simulations which also provide the populations independently. Nevertheless, comparison of populations determined by direct spectral simulation and fitting of SR data with input from simulations provides an internal check on the models.

## 6.1 Dependence of SR Amplitude on NiEDDA Concentration as a Simple Criterion for Exchange Timescale

The most exciting result of the present study is the simple and robust means to identify intermediate exchange: For a spin-labeled mutant that yields a two-component CW spectrum, an initial SR measurement will yield mono- or bi-exponential curves, which in turn indicates a system in fast or intermediate/slow exchange, respectively. To further resolve the exchange timescale in the latter case,  $A_{\text{NF}}$  from direct bi-exponential fits or from UPEN analysis is plotted as a function of RA concentration; a non-zero slope discriminates slow from intermediate (10 kHz–1 MHz) exchange (Fig. 4a). The result of the earlier study of BHH showed that a nonlinearity in a plot of rates of recovery as a function of RA concentration could also be used to identify intermediate exchange, but the nonlinearity is weak and difficult to discern without extremely high quality data over a wide range of RA concentration (Fig. 4b). It should be noted that exchange reagents other than NiEDDA can be used to differentially modulate the relaxation rates of the two spin populations. All that is required is that the “accessibility factor” for the reagent ( $\rho$  in Ref. [32]) that measures solvent accessibility of the more constrained site of R1 be  $\ll 1$ . NiEDDA generally satisfies this condition due to both its polarity and bulk. Oxygen has also been used as a relaxation reagent, but the small size and nonpolar nature result in a much larger accessibility for buried sites. Consequently, there is less discrimination between the exposed (mobile) and more buried (immobile) states with respect to collision, and hence modulation of  $T_1$ s by HE mechanisms [29].



## 6.2 Estimation of Exchange Rates in the 10 kHz–1 MHz Range

As shown in Fig. 4b, the weak nonlinearity of SR rate data on RA concentration makes fitting the corresponding set of SR recovery curves to determine five parameters ( $T_{1\alpha,0}$ ,  $T_{1\beta,0}$ ,  $j_\alpha$ ,  $j_\beta$ ,  $k$ ) problematic [12]. On the other hand, the inclusion of both amplitude and rate data—which have different functional dependencies on the parameters—and globally fitting using amplitude and rate parameters from the UPEN fits to individual relaxation curves provides values for the parameters with relatively low errors (Table 1).

The largest errors in exchange rate constant may arise from uncertainties in the value of  $f_x$  obtained from spectral simulations. Estimates of the uncertainties can be made by simulating the experimental spectra for known mixtures of T4L 131R1 and 121A/133A/130R1 and comparing the value of  $f_x$ , thus determined with the known value. With this approach, the errors are estimated to be  $\leq 10\%$  for both quantities. For experimental systems accessible to the SR approach with resolved mobile and immobile components,  $f_x$  will typically be in the range of 0.2–0.8. Variation of  $f_x$  by 10% within this range in the global fitting procedure can result in changes in the reported values of  $k$  by amounts that depend on the value of  $k$ ; for exchange rates in the middle of the intermediate range, variations are on the order of 20%. For slow exchange near the limit of sensitivity, variation can be as much as a factor of two. Although this is a sizeable uncertainty, it would not result in a fundamentally different view of the role of dynamics in function. The valuable contribution of the SR analysis presented here is to define an approximate timescale for exchange in the 10 kHz–1 MHz range—a timescale difficult to access by other methodologies.

## 7 Summary and Future Directions

A theory for SR amplitudes in systems undergoing two-site exchange is presented, and reveals that the amplitudes depend on more than just the relative populations of the states involved. In particular, the normalized amplitude for the fast relaxing component ( $A_{Nf}$ ) depends on the exchange rate, and in the presence of exchange, is under-represented relative to the true population; the main points of the theory are confirmed experimentally in spin-labeled proteins. The strong dependence of  $A_{Nf}$  on exchange rate provides a robust and simple test for intermediate exchange in the range 10 kHz–1 MHz, and for this application high observing power can be used to substantially reduce data acquisition time. Global analysis of both SR amplitude and rate data permits quantitative evaluation of the exchange rate constant in the above time domain, a timescale difficult for other methodologies.

Recent advances in microwave arbitrary waveform generator (AWG) technology make possible the shaping SR-ELDOR excitation pulses, such that pulse length (time) and frequency span (bandwidth) are no longer inversely coupled within the Fourier bandwidth limit. Using sculpted ‘chirp-pulses’ ensures perfectly rectangular pulse excitation bandwidths for long-pulse SR experiments, while Gaussian shaping allows narrow-bandwidth short pulses with minimal leakage of excitation power to elsewhere in the spectrum. This yields significant advantages for motional

dynamics, spectral editing, and collisional exchange SR-ELDOR studies and evaluation of different pulse shapes for use in these experiments is currently underway.

An important advantage of the SR methods described herein for SDSL is that they can be applied without modification to examine dynamics of conformational exchange in membrane proteins in a native lipid environment and complexes, thereof including those of signal transduction currently under investigation in this laboratory. Recently, it has been shown that SDSL-EPR can detect otherwise “invisible” conformational substates of proteins by the application of high pressure [43, 46, 47]. SR can be used under high pressure with currently available ceramic cells [46], making it possible to explore dynamic excursions between ground and excited states of proteins in future studies. A new challenge is to extend the SDSL-EPR time domain to slower exchange processes, i.e., those with lifetimes in the millisecond regime. Future studies will address this challenge using the high sensitivity of EPR to record real-time exchange using pressure jump methods.

**Acknowledgements** This work was supported by National Institute of Health Grants EY05216, T33 EY07026 and 5P41EB001980, and the Jules Stein Professorship endowment. We are grateful to Profs. Sandra and Gareth Eaton (University of Denver) for providing a UPEN analysis program used early on in the study, and for helpful discussions regarding UPEN theory. We also thank Mark Fleissner, Carlos López, and Evan Brooks for graciously providing some of the spin-labeled mutants reported herein.

## References

1. K. Gunasekaran, B. Ma, R. Nussinov, *Proteins* **57**, 433–443 (2004)
2. V.J. Hilser, J.O. Wrabl, H.N. Motlagh, *Annu. Rev. Biophys.* **41**, 585–609 (2012)
3. L.C. James, P. Roversi, D.S. Tawfik, *Science* **299**, 1362–1367 (2003)
4. O. Keskin, *BMC Struct. Biol.* **7**, 31 (2007)
5. W. Zheng, N.P. Schafer, A. Davtyan, G.A. Papoian, P.G. Wolynes, *Proc. Natl. Acad. Sci. USA* **109**, 19244–19249 (2012)
6. Y. Huang, Z. Liu, *J. Mol. Biol.* **393**, 1143–1159 (2009)
7. K.B. Levin, O. Dym, S. Albeck, S. Magdassi, A.H. Keeble, C. Kleanthous, D.S. Tawfik, *Nat. Struct. Mol. Biol.* **16**, 1049–1055 (2009)
8. W.L. Hubbell, C.J. López, C. Altenbach, Z. Yang, *Curr. Opin. Struct. Biol.* **23**, 725–733 (2013)
9. L. Columbus, T. Kálai, J. Jekö, K. Hideg, W.L. Hubbell, *Biochemistry* **40**, 3828–3846 (2001)
10. L. Columbus, W.L. Hubbell, *Biochemistry* **43**, 7273–7287 (2004)
11. C.J. López, S. Oga, W.L. Hubbell, *Biochemistry* **51**, 6568–6583 (2012)
12. M.D. Bridges, K. Hideg, W.L. Hubbell, *Appl. Magn. Reson.* **37**, 363–390 (2010)
13. M.R. Fleissner, M.D. Bridges, E.K. Brooks, D. Cascio, T. Kálai, K. Hideg, W.L. Hubbell, *Proc. Natl. Acad. Sci. USA* **108**, 16241–16246 (2011)
14. O.F. Lange, N.-A. Lakomek, C. Farès, G.F. Schröder, K.F.A. Walter, S. Becker, J. Meiler, H. Grubmüller, C. Griesinger, B.L. de Groot, *Science* **320**, 1471–1475 (2008)
15. M. Huisjen, J.S. Hyde, *Rev. Sci. Instrum.* **45**, 669–675 (1974)
16. P.W. Percival, J.S. Hyde, *Rev. Sci. Instrum.* **46**, 1522–1529 (1975)
17. H. Sato, S.E. Bottle, J.P. Blinco, A.S. Micallef, G.R. Eaton, S.S. Eaton, *J. Magn. Reson.* **191**, 66–77 (2008)
18. L.I. Horvath, P.J. Brophy, D. Marsh, *J. Magn. Reson. Ser. B* **105**, 120–128 (1994)
19. G.C. Borgia, R.J.S. Brown, P. Fantazzini, *J. Magn. Reson.* **132**, 65–77 (1998)
20. G.C. Borgia, R.J.S. Brown, P. Fantazzini, *J. Magn. Reson.* **147**, 273–285 (2000)
21. G.C. Borgia, R.J.S. Brown, P. Fantazzini, *Magn. Reson. Imaging* **19**, 473–475 (2001)
22. V. Bortolotti, R.J.S. Brown, P. Fantazzini, G. Landi, F. Zama, *Inverse Probl.* **33**, 015003 (2016)
23. S.S. Eaton, G.R. Eaton, *Method Enzymol.* **563**, 37–58 (2015)

24. J.-J. Yin, J.S. Hyde, *J. Chem. Phys.* **91**, 6029–6035 (1989)
25. Z. Yang, M.D. Bridges, M.T. Lerch, C. Altenbach, W.L. Hubbell, *Method Enzymol.* **564**, 3–27 (2015)
26. Z. Yang, M.D. Bridges, C.J. Lopez, O.Y. Rogozhnikova, D.V. Trukhin, E.K. Brooks, V. Tormyshev, H.J. Halpern, W.L. Hubbell, *J. Magn. Reson.* **269**, 50–54 (2016)
27. A. Kusumi, W.K. Subczynski, J.S. Hyde, *Proc. Natl. Acad. Sci. USA* **79**, 1854–1858 (1982)
28. J.M. Isas, R. Langen, H.T. Haigler, W.L. Hubbell, *Biochemistry* **41**, 1464–1473 (2002)
29. C. Altenbach, W. Froncisz, R. Hemker, H. Mchaourab, W.L. Hubbell, *Biophys. J.* **89**, 2103–2112 (2005)
30. Z. Guo, D. Cascio, K. Hideg, W.L. Hubbell, *Protein Sci.* **17**, 228–239 (2008)
31. Z. Guo, D. Cascio, K. Hideg, T. Kálái, W.L. Hubbell, *Protein Sci.* **16**, 1069–1086 (2007)
32. C.J. López, Z. Yang, C. Altenbach, W.L. Hubbell, *Proc. Natl. Acad. Sci. USA* **110**, E4306–E4315 (2013)
33. C.J. López, M.R. Fleissner, Z. Guo, A.K. Kusnetzow, W.L. Hubbell, *Protein Sci.* **18**, 1637–1652 (2009)
34. K. Joon Oh, C. Altenbach, R.J. Collier, W. Hubbell, in *Bacterial Toxins: Methods and Protocols*, ed. by O. Holst (Humana Press, New York, 2000), pp. 147–169
35. W.L. Hubbell, W. Froncisz, J.S. Hyde, *Rev. Sci. Instrum.* **58**, 1879–1886 (1987)
36. P.W. Percival, J.S. Hyde, *J. Magn. Reson.* **23**, 249–257 (1976)
37. J.S. Hyde, in *Time Domain Electron Spin Resonance*, ed. by L. Kevan, R.N. Schwartz (Wiley, New York, 1979), pp. 1–30
38. D.E. Budil, S. Lee, S. Saxena, J.H. Freed, *J. Magn. Reson. Ser. A* **120**, 155–189 (1996)
39. A.K. Kusnetzow, C. Altenbach, W.L. Hubbell, *Biochemistry* **45**, 5538–5550 (2006)
40. M.R. Fleissner, D. Cascio, W.L. Hubbell, *Protein Sci.* **18**, 893–908 (2009)
41. M.R. Fleissner, Ph.D. Thesis, University of California, Los Angeles, 2007
42. M.E. Hodsdon, D.P. Cistola, *Biochemistry* **36**, 2278–2290 (1997)
43. J. McCoy, W.L. Hubbell, *Proc. Natl. Acad. Sci. USA* **108**, 1331–1336 (2011)
44. C. Altenbach, W. Froncisz, J.S. Hyde, W.L. Hubbell, *Biophys. J.* **56**, 1183–1191 (1989)
45. J. Pyka, J. Ilnicki, C. Altenbach, W.L. Hubbell, W. Froncisz, *Biophys. J.* **89**, 2059–2068 (2005)
46. M.T. Lerch, J. Horwitz, J. McCoy, W.L. Hubbell, *Proc. Natl. Acad. Sci. USA* **110**, E4714–E4722 (2013)
47. M.T. Lerch, Z. Yang, E.K. Brooks, W.L. Hubbell, *Proc. Natl. Acad. Sci. USA* **111**, E1201–E1210 (2014)